energies

MDPI

Review

Photocatalytic Evolution of Hydrogen Peroxide: A Minireview

Nikolaos Karamoschos [1] and Dimitrios Tasis [1,2,*]

[1] Department of Chemistry, University of Ioannina, 45110 Ioannina, Greece
[2] University Research Center of Ioannina (URCI), Institute of Materials Science and Computing, 45110 Ioannina, Greece
* Correspondence: dtassis@uoi.gr

Abstract: Hydrogen peroxide (H_2O_2) has demonstrated applicability in a wide range of applications, spanning from a bleaching agent in the pulp industry, environmental remediation, and fuel cell technology. Industrial scale synthesis, either by the anthraquinone method or catalytic oxidation of hydrogen gas, has serious drawbacks which are related with energy demanding and multi-step processes. An alternative green strategy involves the photocatalytic synthesis of H_2O_2. All that is needed is the renewable energy of the sun, a semiconducting species absorbing in the visible region, water, and oxygen. In this minireview, we describe the evolution of research milestones that have been achieved within the recent decades regarding the development of functional photocatalytic systems. In the early studies, back in the 1980's, TiO_2-based systems were mostly investigated. However, due to the large band gap of titania (3.2 eV), alternative semiconductors were studied which strongly absorb in the visible region. Thus, a variety of semiconductor families have been investigated, such as doped titania systems, other metal oxides, metal sulfides, organic semiconductors, metal-organic frameworks, carbon nitride systems, etc. In parallel, the development of functional dopants onto the surface of the main semiconductor has lead to both the inhibition of electron-hole recombination and H_2O_2 degradation. The current minireview collectively provides the studies of the higher H_2O_2 production rates and offer some suggestions for the near future.

Keywords: photocatalysis; hydrogen peroxide; semiconductor; oxygen reduction; water oxidation

Citation: Karamoschos, N.; Tasis, D. Photocatalytic Evolution of Hydrogen Peroxide: A Minireview. *Energies* **2022**, *15*, 6202. https://doi.org/10.3390/en15176202

Received: 11 August 2022
Accepted: 23 August 2022
Published: 26 August 2022

1. Introduction

Photocatalytic processes have been recognized as an alternative approach towards the achievement of a variety of chemical transformations [1]. The latter are related with a wide range of applications, including issues that are related to the environment (degradation of polluting species) [2] as well as energy conversion (synthesis of "green" fuels) [3]. The photocatalytic transformations take place through the redox reactions of either holes or electrons of photoexcited semiconducting species. Both oxidative and reductive paths result in the generation of either reactive species or neutral substances. In many cases, aqueous systems in an oxygen atmosphere are used in photocatalytic processes, so oxygen-based photo-adducts are expected to be formed. The main reactive oxygen species are hydroxyl radicals, singlet oxygen, superoxide anion radical, and hydrogen peroxide. In photocatalysis, the driving force towards high-yield half-reactions depends on the energy difference between either the conduction or valence band of the photocatalyst with the corresponding potentials of the half reactions [4].

Hydrogen peroxide (H_2O_2) is considered as a green oxidant for either organic or inorganic structures. Regarding the synthetic strategies of hydrogen peroxide, an increased interest has been given by researchers, since the substance is considered both as a promising fuel as well as an environmentally friendly substance towards oxidative synthetic approaches [5]. Regarding the utilization as a potential fuel, this is supported by the fact that its transportation and storage are relatively safe processes due to the physical state of the substance (liquid) at ambient conditions. Since the side products in its reactions are not

dangerous (oxygen and water), H_2O_2 has been widely applied as a bleaching agent in the paper industry [6] or in wastewater treatment [7].

Until now, an energy-demanding multi-step industrial approach has been widely utilized towards the synthesis of H_2O_2, the so-called anthraquinone (AQ) process [8]. This approach involves a combination of energy-demanding chemical reactions, extraction steps by harmful organic media, and thus, the production of unwanted wastes. This multistep process cannot be considered as a green technology protocol. Thus, alternative green strategies need to be developed in order to synthesize hydrogen peroxide in large quantities, without harming the environment. In the recent decades or so, an alternative synthetic process involves the direct compounding of hydrogen and oxygen gases in the presence of a nanostructured catalyst. It is noted that the noble metals (or its alloys) that are used as catalytic systems increase the cost of the protocol drastically. Some of the nanostructured metals possess active crystallographic planes, which catalyze the decomposition of H_2O_2. This leads to lower production rates of the oxidant substance. Furthermore, the catalyst-based reactions of hydrogen and oxygen gases often result in an explosion, thus, it is imperative to purge the reactor with an inert gas (Ar, N_2, etc.). All the aforementioned drawbacks have restricted the applicability of the process on the industrial scale. Alternative approaches by using renewable energy sources have been developed in the last 20 years or so. Specifically, hydrogen peroxide synthesis has been accomplished through photoexcitation of semiconductor-based systems in an oxygen-saturated atmosphere [9]. Due to the environmentally friendly character of the process, the photocatalytic synthesis of H_2O_2 has attracted great interest and this is reflected by the huge production of related publications. Therefore, the timing is correct in order to demonstrate the current progress that has been achieved in the development of functional catalytic systems for the photosynthesis of H_2O_2.

In this review, we first describe the photocatalytic paths that were suggested to take place during the synthesis of H_2O_2 in some seminal works. Subsequently, we discuss the various photocatalytic systems that have been used so far for the aforementioned synthetic transformation. In addition, some comparative data are illustrated within a comparative Table, in which the most efficient photocatalytic systems have been selected. The review aims to demonstrate the current status in the literature and even propose new avenues to the development of functional photocatalytic systems.

2. Redox Reactions during Photocatalytic Synthesis of H_2O_2–Early Considerations

Semiconductor-based photocatalytic reactions include three main processes [10]. Firstly, absorption of photon energy takes place by the semiconducting species. Great caution should be given to the energy band gap of the semiconductor and the amount of incident light in order to achieve a successful excitation. The first step results in the enrichment of the conduction band by electrons and the valence band by holes. The photoinduced electrons and holes separate from their bound state (exciton) and escape to the surface of the nanostructured semiconductor. The aforementioned carriers may react with a variety of species in the interfacial region between the semiconductor surface and the adjacent liquid environment. As a competitive process, the recombination of electrons and holes may take place, resulting in low efficiency photocatalytic reactions.

The basic principles of photocatalysis stand also for the synthesis of H_2O_2. In total, the aforementioned substance may be generated through either two-electron reduction of oxygen or two-hole oxidation of water. Starting from the reductive path and specifically through the oxygen radical anion species ($^{\bullet}O_2^-$), the following two reduction paths are valid:

$$O_2^- + {}^{\bullet}O_2H + H_2O \rightarrow H_2O_2 + O_2 + OH^-$$

$$O_2^- + e^- + 2H^+ \rightarrow H_2O_2$$

The former involves the so-called disproportionation reaction, whereas the latter involves the participation of conduction band electrons. Other than the reductive path,

the hole-mediated oxidation of water may take place. This can be described in the following equation:

$$2H_2O + 2h^+ \rightarrow H_2O_2 + 2H^+$$

The aforementioned oxidative reaction may be further divided in two process, one hole-mediated and the other which is considered as dimerization.

$$H_2O + h^+ \rightarrow HO^\bullet + H^+$$

$$2HO^\bullet \rightarrow H_2O_2$$

The seminal studies in the photoinduced synthesis of H_2O_2 involved mainly the utilization of TiO_2 aqueous suspensions as the environment for hydrogen peroxide generation. As stated previously, such photoinduced synthetic processes may result in either reductive or oxidative paths. In the former case, the peroxide may be formed by a stepwise reduction of dissolved oxygen gas, in which two electrons are consumed in total [11]. The intermediate species that is formed is an oxygen radical anion. In parallel, a direct one-step reduction of oxygen takes place under a two-electron mechanism.

Early studies suggested that H_2O_2 was solely formed by reductive paths of photoexcited TiO_2 through the oxygen radical anion species [12]. The authors observed that no H_2O_2 was formed under inert atmosphere (nitrogen-purged solution), implying that H_2O_2 was generated from the reduction site of the photocatalyst, its conduction band. Furthermore, the presence of Cu^{2+} ions was found to act catalytically towards the enhanced generation of H_2O_2 by the following reactions:

$$O_2^- + Cu(II) \rightarrow O_2 + Cu(I)$$

$$O_2^- + 2H^+ + Cu(I) \rightarrow H_2O_2 + Cu(II)$$

Different conclusions were drawn by Diesen et al. [13] concerning the generation of H_2O_2 in a de-aerated environment. The authors concluded that the peroxide was generated through the dimerization of hydroxyl radicals at such conditions. To further elucidate the origin of the H_2O_2, radical trapping experiments were conducted by using the radical scavenger tris(hydroxymethyl) aminomethane (Tris). The results showed that, in a deoxygenated system, no H_2O_2 could be detected due to hydroxyl radical scavenging by the Tris reagent. This experiment actually supported the suggestion of the authors that H_2O_2 formation took place by the dimerization of the hydroxyl radicals.

As stated previously, the oxidative character of the holes may result in redox transformations of water substance. These include either the oxidation of water to O_2 (four-hole mechanism), the oxidation of water to H_2O_2 (two-hole mechanism) [14], or the oxidative transformation of water to hydroxyl radicals, which may be dimerized in order to form H_2O_2.

3. Functional Photocatalytic Systems for H_2O_2 Evolution

3.1. Titanium Dioxide (TiO_2)

The photocatalyst which has been studied most in depth is titanium dioxide (titania, TiO_2). The aforementioned semiconductor demonstrates enhanced photostability, biocompatibility, yet its large band gap results in a negligible absorption to visible light wavelengths. The photocatalytic production of H_2O_2 in aqueous TiO_2 suspensions has been studied in the seminal work of Hoffmann and co-workers, back in 1988 [15]. It was found that an appreciable amount of peroxide was detected in the presence of electron donors such as acetates. The latter were oxidized by the holes in the valence band of a semiconductor, interfering with the recombination inhibiting step. Beside H_2O_2, organic peroxides were formed, such as CH_3OOH and CH_3OOCH_3. Kinetic analysis of the H_2O_2 production rate revealed that after 5 min irradiation with 350 nm light source, a concentration of 0.9 μM was estimated.

Analogous results were found in the work of Goto et al. [16]. The authors used isopropanol as a hole scavenger, so that the oxidative generation of H_2O_2 was inhibited efficiently. The reduction products from molecular oxygen were found to be different, depending on the crystal lattice of titania photocatalyst. It was demonstrated that the main product was a superoxide ion when rutile particles are used, whereas hydrogen peroxide was mainly generated when anatase particles were used as the photocatalyst. Furthermore, it was found that the utilization of isopropanol as a hole scavenger rules out the scenario of the oxidative production of H_2O_2. Mechanistic investigation exhibited some interaction between isopropanol and superoxide ions towards the formation of acetone and hydrogen peroxide.

Hydrogen peroxide evolution, formed through a reductive strategy was attempted by the work of Selli and co-workers [17]. The hole scavengers that were used were formic acid and benzoic acid, respectively. The degradation rate of both hole scavengers was maximum at pH 4.2 and decreased either at lower or higher pH values. The observed trends were correlated with the electrostatic interactions between the substrate and the photocatalyst surface at different acidity ranges. In the case of formic acid photodegradation, no appreciable amount of hydrogen peroxide was formed. The authors attributed this result to the fact that the TiO_2 surface was not significantly protected by adsorbed formic acid molecules. This could result in the formation of Ti–peroxo complexes (Ti^{IV}-OOH). Electron transfer processes, induced by photogenerated species, may lead to either the reduction or oxidation of the peroxo function.

The tendency of aromatic hole scavengers to contribute to more enhanced hydrogen peroxide yields when compared with aliphatic ones, was also shown by other works. The utilization of aromatic alcohols as efficient hole scavengers towards the generation of high yield hydrogen peroxide was demonstrated by Shiraishi et al. [18]. The irradiation of titania suspensions in the presence of a benzylic alcohol under an oxygen atmosphere resulted in the generation of H_2O_2 at a concentration of 40 mM. The enhanced H_2O_2 yield was suggested to be due to the efficient formation of side-on coordinated peroxo species on the semiconductor surface that were produced via the reaction of benzylic alcohols and O_2 in water. Such peroxo functions consist of three-membered rings of one Ti^{4+} and two oxygen atoms. The utilization of benzaldehyde as a hole scavenger was not effective for H_2O_2 formation, nor was the visible light irradiation of benzylic alcohol-containing suspensions.

By using visible light irradiation, heteroatom-doped titania was studied as photocatalysts for the selective synthesis of either oxygen radical anions or hydrogen peroxide [19]. The authors demonstrated that the sulfur-doped TiO_2 surpassed the N-doped TiO_2 in the ability to produce oxygen radical anions, while the N-doped TiO_2 surpassed the S-doped TiO_2 in producing hydrogen peroxide. The different behavior in the photocatalytic processes was attributed to the multivalence character of the sulfur moieties, which may promote the decomposition of H_2O_2. Visible light irradiation for 10 min gave rise to an H_2O_2 concentration of 0.055 μM by using the N-doped TiO_2 system. The corresponding value for the S-doped material was below 0.01 μM.

An efficient production of H_2O_2 was demonstrated by Xiao and co-workers through a two-step hydrothermal process in autoclave conditions (Figure 1) [20]. In the first step, the authors treated commercial P25 TiO_2 nanoparticles in an alkaline aqueous medium under hydrothermal conditions. The TiO_2 nanotubes (TNT) were isolated bearing Na^+ as counterions. By an ion-exchange process, the sodium ions were replaced by protons in order to acquire the adduct HTNT. In a subsequent step, the latter adduct was mixed with citric acid (CA) and the whole mixture was hydrothermally treated in order to obtain a hybrid assembly of HTNT and carbon dots (CD). Irradiation under visible light resulted in an H_2O_2 production rate of 4.8 mM/h. The presence of acidic protons on the TNT surface was crucial for the acceleration of the reaction between molecular oxygen and electrons towards the formation of H_2O_2. It is noted that irradiation with a source emitting at $\lambda > 365$ nm demonstrated decreased H_2O_2 yields, when compared with the values that were acquired at the first two hours of irradiation.

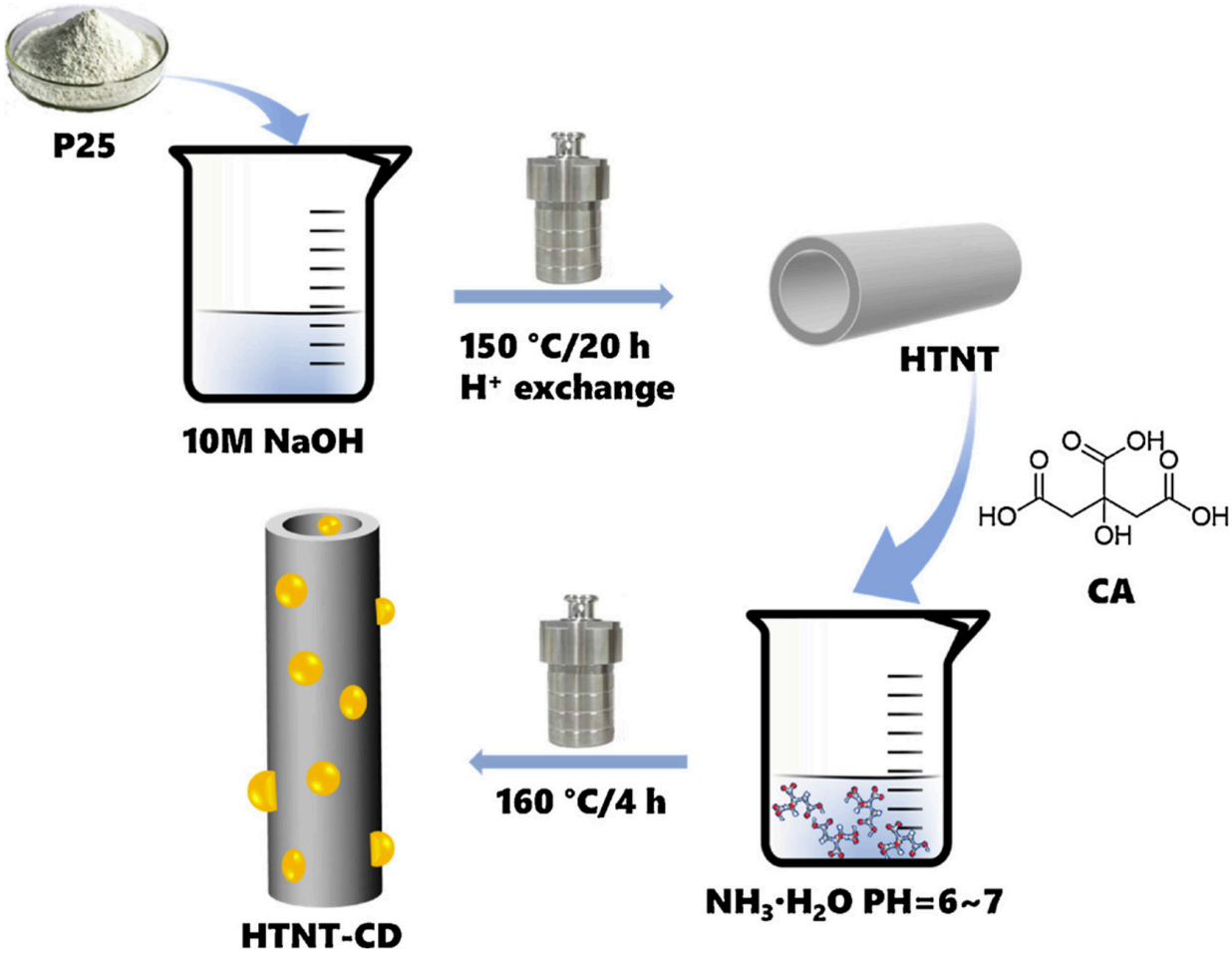

Figure 1. Synthetic sequence for the preparation of HTNT-CD assembly. Adapted with permission from Ref. [20]. Copyright 2019 Elsevier.

In an analogous study, the coating of both heteroatom-doped graphitic nanostructures (N,S-codoped graphene dots) and anionic perfluorosulfonic polymer (Nafion) onto nanostructured TiO_2 surface resulted in the enhanced generation of H_2O_2 [21]. The hybrid demonstrated much higher photocatalytic activity under simulated sunlight irradiation, than in the case of visible light. In the latter case, the dual-doped graphene dots acted as potential photosensitizer, contributing to the electronic enrichment of a TiO_2 conduction band. Regarding the simulated sunlight irradiation, the optimized hybrid (5% Nafion-SNGr@TiO_2) demonstrated an H_2O_2 production of 745 μM within 2 h of irradiation. The authors suggested that the Nafion layer on the TiO_2 surface accelerated the oxygen diffusion from the liquid medium for electron scavenging. In parallel, the available protons on the catalyst surface increased in the presence of an anionic polymer coating. Nafion loading that was higher than 5 wt% gave rise to lower H_2O_2 production rates. This could be explained due to excessive coverage of the semiconductor surface, making the physical adsorption of hole scavengers impossible.

In an alternative approach, TiO_2@carbon composites were prepared by carbonization of aromatic compounds that were adsorbed onto the surface of inorganic oxide [22]. Specifically, pyrolytic decarboxylation of either benzoic acid or 1-naphthoic acid resulted in the synthesis of core-shell TiO_2@carbon hybrids. The pyrolytic process was suggested to generate aryl radicals, which react either with similar species or aromatic carboxylic acids with the subsequent formation of a protecting carbon layer. The naphthoic acid-derived hybrid contained a larger population of oxygenated groups, with the latter being predominantly epoxide rings. The sp^2-hybridized domains near the epoxide groups were

found to act as catalytic sites for the two-electron reduction of oxygen, thus, making the naphthoic-acid-derived hybrid a more efficient photocatalyst.

Covalent immobilization of polyoxometalates $(PW_9O_{24})^{9-}$ onto TiO_2 was demonstrated by Wu et al. [23]. The hydrothermally synthesized TiO_2-polyoxometalate photocatalyst demonstrated higher efficiency for H_2O_2 generation than the corresponding one of hybrid, prepared by the physical mixing of the components. By using benzyl alcohol as a hole scavenger, the photocatalytic system generated about 38 μmol H_2O_2 within two hours of irradiation. The attachment of polyoxometalate clusters in the hybrid was suggested to lead to enhanced light absorption and charge carrier transport. The material which has been recycled four times has shown similar activity regarding the H_2O_2 yield.

3.2. Metal Nanoparticle-Decorated Titania

In most of the aforementioned studies, the H_2O_2 yield was in the micromolar scale. The low yield was ascribed to the reaction of H_2O_2 with surface Ti-OH groups, resulting in the formation of surface peroxide species. The latter were found to be reduced by the excited electrons of the semiconductor conduction band. A versatile approach by which the H_2O_2 degradation may be inhibited is the displacement of hydroxyl moieties of the TiO_2 surface by other ions, such as F^- [24]. The production of H_2O_2 at a millimolar scale was achieved as a consequence of the suppression of the degradation reaction. The H_2O_2 formation rate was fully consistent with the surface speciation, acquiring the maximum value when the whole population of hydroxyls was displaced by fluorides.

Besides the displacement of surface hydroxyl moieties, decoration of the TiO_2 surface by metal cocatalyst nanoparticles was studied in detail. The enhanced photoactivity stems from the interfacial electron transfer between TiO_2 and a metal cocatalyst. The latter process gives rise to efficient carrier separation, whereas the oxidation sites (TiO_2 surface) and reduction sites (metal nanoparticle surface) are spatially separated. Teranishi et al. [25] have demonstrated the drastic enhancement of H_2O_2 generation by TiO_2 that is loaded with Au nanoparticles. By using ethanol as a hole scavenger, the hybrid photocatalyst was able to photogenerate H_2O_2 on an 8 mM level under UV irradiation for 24 h. The most efficient activity appeared for the hybrids containing Au nanoparticles of diameter in the range between 7 and 8 nm. Although the Au nanoparticles act as an efficient catalytic site for two-electron reduction of O_2, an additional side-reaction may occur in strongly adsorbed H_2O_2 molecules. The latter may be reduced on the metal surface, giving hydroxyl radicals and anions, respectively. Thus, Au particles promote the formation and catalyze the decomposition of H_2O_2, simultaneously.

Furthermore, the same group studied the effects of both temperature and pH on the yield of H_2O_2 [26]. It was found that as the temperature and pH of the solution decreased, the H_2O_2 generation was enhanced. At 5 °C and pH 2, the yield of H_2O_2 reached the value of 17 mM after 23 h of irradiation. The quantum efficiency for H_2O_2 formation was estimated to be 22% by assuming a two-electron mechanistic scheme. The authors suggested that H_2O_2 was preferentially grown onto the Au surface, which strongly supports the avoidance of the decomposition process onto the TiO_2 surface. In order to inhibit the undesired side-reaction of H_2O_2 decomposition through the formation of Ti-OOH species, Shiraishi and coworkers [27] have synthesized TiO_2 that is loaded with AuAg bimetallic alloy nanoparticles. The reason for the study of the alloy-based system was that the formed H_2O_2 could be adsorbed onto the neat Au surface and decompose via a reductive path towards the generation of hydroxy radicals and anions, respectively. UV photoirradiation for 12 h of Au/TiO_2 afforded 1.5 mM H_2O_2, whereas the utilization of the alloy as a cocatalyst resulted in the highest photocatalytic activity, yielding 3.4 mM of H_2O_2. It was found that the double effect of the alloy particles involved both the carrier separation in the TiO_2/alloy interface as well as the decreased H_2O_2 adsorption onto the Au nanoparticles.

Analogous TiO_2/Au nanostructures were grown onto silicon nanowires by a combination of molecular layer deposition, thermal annealing, and liquid phase reduction protocols [28]. The photocatalytic production of H_2O_2 took place without the need of

sacrificial organic substances and reached a plateau at about 15 h of irradiation with a 365 nm light source. The maximum concentration of H_2O_2 was estimated at 38 μM.

Solid-phase photocatalytic films of TiO_2/Au onto glass substrate showed an enhanced yield of H_2O_2 formation (Figure 2) [29]. The TiO_2 film was deposited by spin coating, followed by calcination at 550 °C in order to acquire porosity. The Au nanoislands were deposited using a thermal or e-beam evaporation, with a size ranging between 2 and 20 nm. The enhanced photocatalytic activity was attributed to the co-existence of both small- and large-size Au nanoislands, which possess size-dependent work functions, thus minimizing the recombination of electron-hole pairs. After 20 min of irradiation, the H_2O_2 yield reached a value of 1.5 mM. The performance enhancement was about 80 times higher than the one of neat TiO_2.

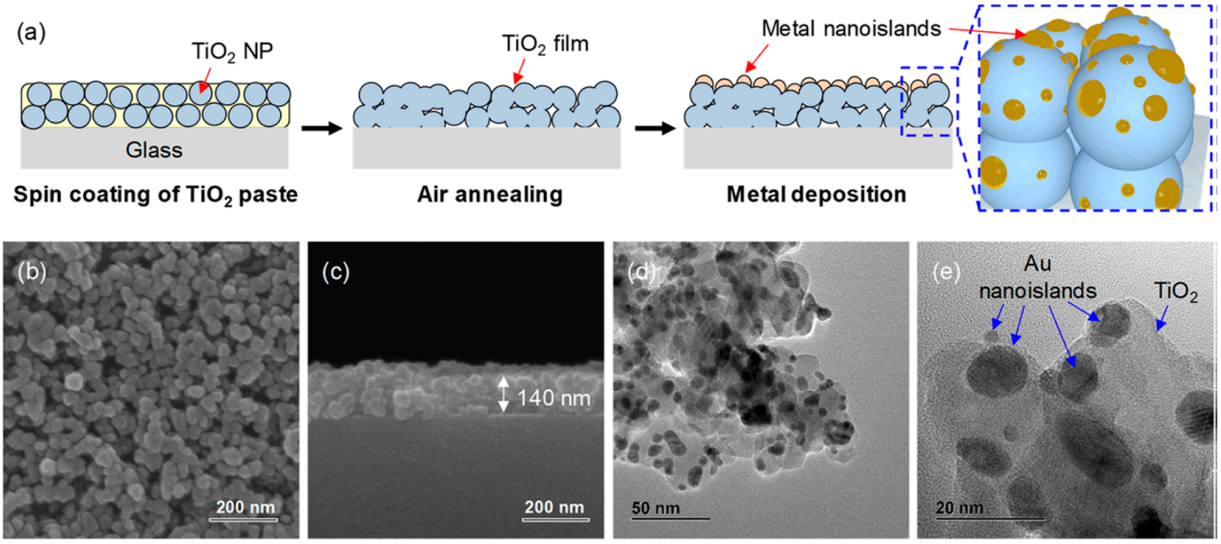

Figure 2. (**a**) Schematic illustration of the fabrication process for the solid-phase photocatalytic films. (**b**,**c**) Top and cross-sectional SEM images of annealed TiO_2 films. (**d**,**e**) TEM images of Au/TiO_2 hybrid. Adapted with permission from Ref. [29]. Copyright 2019 ACS.

An alternative passivation component for the inhibition of H_2O_2 degradation onto a TiO_2 surface involves tin oxide (SnO_2) [30]. The SnO_2/TiO_2 heterostructure, prepared by annealing at 500 °C, demonstrated the best performance. Decoration of the hybrid with 0.1 wt% Au resulted in an H_2O_2 yield of about 16 mM after 26 h of irradiation. The SnO_2 passivation layer was responsible for the inhibition of H_2O_2 decomposition. An optimal SnO_2 content was 4 wt%, while an excess oxide content was suggested to cause a shielding effect on the photo-absorption of the main semiconductor, TiO_2. Similar three-component hybrids were prepared by a liquid-phase compounding protocol [31]. SnO_2 nanorods were grown under autoclave conditions at 180 °C. Photoexcitation under visible light resulted in an H_2O_2 production rate of about 60 μM within 6 h.

3.3. Other Oxides

Besides using titania-based hybrids as the photocatalytic system for H_2O_2 formation, the group of Hoffmann studied the activity of ZnO under ultraviolet irradiation [32]. In the presence of organic acids as the hole scavengers, aqueous ZnO suspensions were shown to generate H_2O_2 concentrations up to 2 mM. The order of efficiency of hole scavengers was as follows: formate > oxalate > acetate > citrate. The suggested mechanism for the oxidative decomposition of hole scavengers involved the generation of methyl radicals and carbon dioxide, in the case of acetate anion. Isotopic labeling investigation demonstrated that all the oxygen in the H_2O_2 adduct originated from molecular oxygen gas. In an analogous study, immobilized ZnO nanorod arrays were used as a photocatalyst for H_2O_2 generation [33]. The formation rate depended on the synthetic conditions of the ZnO

nanorods, namely the starting concentrations of the precursor substances. The maximum concentration of H_2O_2 that was achieved was about 1.5 μM, after 6 h of UV irradiation.

By using visible wavelengths for excitation, Shiraishi and co-workers [34] have assessed the photocatalytic performance of $BiVO_4$@Au hybrids for H_2O_2 formation. After a 10 h irradiation, the H_2O_2 yield reached a concentration of about 40 μM in pure water. Due to the favorable band alignment between the $BiVO_4$ conduction band and the one- and two-electron reduction potentials of oxygen species, the photoexcitation of the hybrids selectively promoted the generation of H_2O_2 by the two-electron mechanism. Furthermore, a fraction of H_2O_2 was also originated from water oxidation, which was supported by appropriate photocatalytic experiments by using $AgNO_3$ as an electron acceptor.

Tada and co-workers [35] have studied the utilization of photocatalysts consisting of $BiVO_4$ and Cu(II) complexes. Visible light irradiation in the presence of ethanol as a hole scavenger demonstrated that the presence of copper bis(acetonato)-type complexes was crucial towards the enhancement of photocatalytic performance. The positive contribution was attributed to the charge separation enhancement from $BiVO_4$ to the complex structure. The H_2O_2 yield was up to 120 μM after 90 min of irradiation. No apparent decay of the photocatalytic activity was observed after five cycles. In the absence of a sacrificial agent, the corresponding production rate was 58 μM/h, yet the degradation of the copper complex took place simultaneously.

An alternative electron bridge component that was compounded with $BiVO_4$ nanostructures was reduced graphene oxide (rGO) (Figure 3) [36]. The latter nanostructure may induce efficient electron transfer due to its extended conjugate network of sp^2-hybridized carbon atoms. The synthetic protocol was based on an electrostatic self-assembly approach, by using a precursor state of rGO, the graphene oxide.

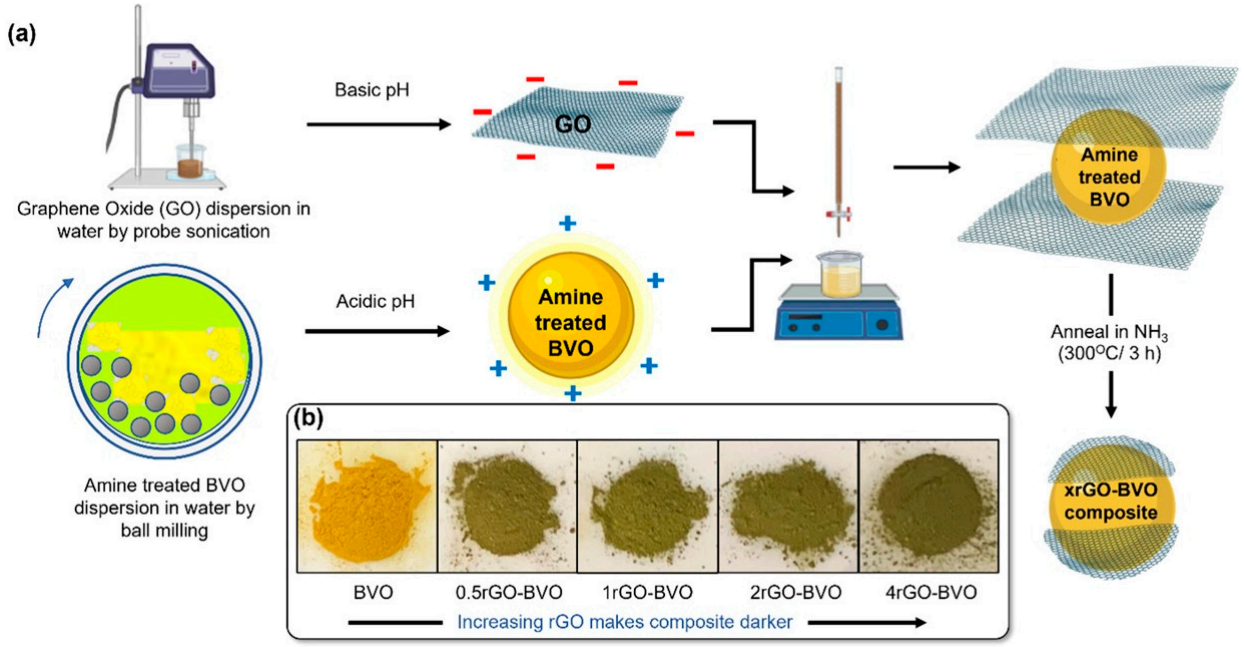

Figure 3. (**a**) Encapsulation of $BiVO_4$ with graphene oxide flakes and subsequent annealing to rGO. (**b**) Digital photos of powders of neat $BiVO_4$ and hybrids with variable rGO mass loading. Adapted with permission from Ref. [36]. Copyright 2021 ACS.

The maximum H_2O_2 yield reached a value of 300 μM after a 2 h irradiation process. The optimal production rate was achieved in a rGO loading of 1 wt%. Higher loading led to the lowering of the H_2O_2 yield. This was attributed either to a shielding effect to the photo-absorption or blocking of the semiconductor active sites. Another form of mixed metal oxide nanostructures as potentially active photocatalysts includes the nickel titanate ($NiTiO_3$), which was synthesized by a hydrothermal strategy [37]. The maximum

concentration of H_2O_2 reached 2.5 mM when nickel titanate was irradiated for 1 h in an oxygen-saturated aqueous suspension. The data suggested that H_2O_2 was formed by either photogenerated electrons or holes. This could be explained by performing the following two experiments: (a) saturation of the medium with an inert gas gave rise to a decreased H_2O_2 yield; (b) a further decrease was observed by using methanol as a hole scavenger in a nitrogen-saturated environment.

Hollow MoO_3@SnS_2 nanotubes were synthesized by a two-step hydrothermal treatment at moderate temperatures [38]. Hydrogen peroxide was rapidly formed over the hybrid catalyst surface, reaching 100 μM within 100 min of irradiation. The corresponding activity of the hybrid that was prepared by physical mixing of the components was relatively lower (about 10 μM), implying their close contact in the hydrothermally prepared hybrid. Photocatalytic experiments were held in the presence of both hydroxy radical and oxygen radical anion scavengers, demonstrating a 90% decrease of the H_2O_2 yield. The hybrid demonstrated enhanced photostability after four cycles of testing.

3.4. Metal Sulfides

Lee and co-workers [39] demonstrated the sustainable synthesis of H_2O_2 in the absence of organic hole scavengers by a CdS-reduced graphene oxide (rGO) photocatalyst in sunlight with water and oxygen as resources. Under hydrothermal conditions, hybrids were prepared with a maximum rGO content at 30 wt%. The sample containing 20 wt% rGO showed optimum photocatalytic activity, which was five times higher than the one of neat CdS after 12 h irradiation.

By using a synchronous crystallization at room temperature, Zhang et al. [40] have synthesized Co_9S_8/Mn_3O_4 hybrids. The adoption of Z-scheme irradiation gave rise to enhanced separation of the carriers (electrons and holes). An optimal photocatalytic system generated a maximum 1.6 mM of H_2O_2 after 6 h irradiation, without using hole scavenger and purging pure oxygen gas. The Z-scheme contributed to the fact that the electrons in the conduction band of Co_9S_8 were the reducing agents for oxygen transformation by a two-electron mechanism, whereas the holes in the valence band of Mn_3O_4 generated a relatively high population of hydroxyl radicals, through which additional H_2O_2 could be produced.

Tian et al. [41] have synthesized zirconium trisulfide (ZrS_3) nanobelts, containing defect sites such as disulfide (S_2^{2-}) and sulfide anion (S^{2-}). Such vacancies exhibited optimal photocatalytic performance. The H_2O_2 generation was coupled with simultaneous benzylamine oxidation. The utilization of defective ZrS_3 nanobelts yielded an enhanced H_2O_2 generation rate of 78 μmol/h, under a simulated sunlight irradiation.

Kang and co-workers [42] have developed an SnS_2/In_2S_3 Type II heterostructure, coupled with carbon dots (CD). In this system, CD were suggested to act as an electron sink, regulate the kinetics of the carriers in the heterojunction, and then further increase the electron–hole separation efficiency of the SnS_2/In_2S_3/CD hybrid. On the other hand, CD were considered as the photo-active sites for the oxygen reduction to H_2O_2. The hybrid heterostructure displayed superior activity with a H_2O_2 yield of about 1112 $\mu mol \cdot h^{-1} \cdot g^{-1}$.

3.5. Metal-Organic Frameworks (MOFs)

Metal-organic frameworks, consisting of metal cation species and organic linkers, have been shown to act as potential photocatalytic systems for the generation of hydrogen peroxide [43]. Yamashita and co-workers [44] synthesized an MOF that was composed of $Ti_8O_8(OH)_4$ clusters and 2-aminoterephthalic acid, MIL-125-NH_2, which was applied for photocatalytic H_2O_2 synthesis due to its visible light absorption. The photoactivity stems from the ligand-to-cluster charge transfer transition. The authors studied the oxygen reduction reaction by the radical anion of the Ti-based cluster in the presence of benzyl alcohol which acted as hole scavenger. Furthermore, it was concluded that the catalytic activity could be greatly enhanced by the deposition of nickel oxide nanoparticles onto the MOF structure. The metal oxide was suggested to accelerate the H_2O_2 formation through

disproportionation of the oxygen radical anion. After 8 h of irradiation, the H_2O_2 yield was about 8 mM in the NiO/MOF hybrid.

In a similar study, Yu and co-workers [45] have fabricated MIL-125-NH_2@ZnS heterostructures by a two-step solution-phase protocol. The optimized MIL-125-NH_2@ZnS hybrid demonstrated a high photocatalytic activity for O_2 reduction with an H_2O_2 production rate of about 120 mM/g/h. It was concluded that heterojunction coverage plays a crucial role in the regulation of the photocatalytic properties of hybrid nanostructures.

Analogous studies with the same MOF, modified with a hydrophobic aliphatic substance, were carried out in a biphasic system of benzyl alcohol/water (Figure 4) [46,47]. In the amino functionality of the MOF structure, a number of hydrophobic chains were attached through an amidation reaction [46]. After a 3 h irradiation, the H_2O_2 yield was estimated to reach values up to 15 mM. The catalyst activity was found to be strongly dependent on the relative volume of water as well as the pH of the aqueous environment. In the case of using an organophosphonic acid (OPA) as a hydrophobic agent, the activity enhancement was attributed to the preservation of the access of the inner pores, due to the selective adsorption of the hydrophobic chain to the outermost surface of the MOF structure [47]. The oxidation adduct, benzaldehyde, was selectively diluted in the organic phase, whereas H_2O_2 to the aqueous phase. After a 3 h irradiation, the H_2O_2 yield was estimated to be about 1.3 mM.

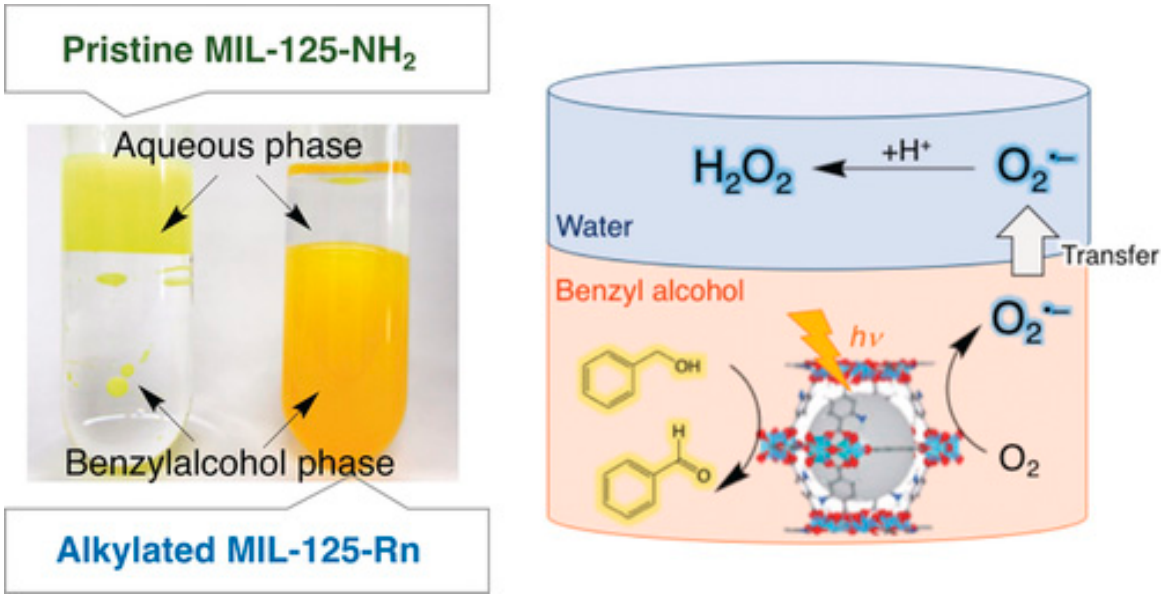

Figure 4. (**Left**) Digital pictures of two-phase systems that were composed of an aqueous phase and benzylalcohol phase containing neat MIL-125-NH_2 and the corresponding MOF, modified with a hydrophobic aliphatic substance. (**Right**) Photocatalytic H_2O_2 production utilizing the two-phase system. Adapted with permission from Ref. [46]. Copyright 2019 Wiley-VCH.

Furthermore, in situ synthesis of MIL-125 MOF was accomplished in the presence of 4,4′,4″,4‴-(pyrene-1,3,6,8-tetrayl) tetrabenzoic acid linker [48]. Due to the introduction of the ligand, the morphology of MOF crystallites contained more structural defects and possessed slightly larger BET surface areas and pore volumes. The most efficient photocatalyst accomplished a remarkable H_2O_2 production rate of 1654 μM/h under visible-light irradiation ($\lambda > 400$ nm) using triethanolamine as a hole scavenger.

Ti-doped zirconium (2-amino terephthalic acid) MOF structures, modified by an organophosphonic acid, demonstrated an even higher photocatalytic activity towards the generation of H_2O_2 in a biphasic system [49]. The hydrophobic OPA/$Zr_{92.5}Ti_{7.5}$-MOF exhibited a remarkable H_2O_2 production rate of 9.7 mM/h under the irradiation of visible light ($\lambda > 420$ nm), which was about 4.5 times higher than that of the parent zirconium-based MOF (Zr_{100}-MOF). The enhanced activity was attributed to the effective Ti-doping, which

played the role of effectively promoting the charge transfer from photoexcited linkers of MOF, inhibiting the recombination of photogenerated electron-hole pairs.

3.6. Carbon-Based Semiconductors

Semiconducting low molecular weight substances, such as biscoumarin-containing acenes, have been used as potential photocatalysts for H_2O_2 generation [50]. Visible light irradiation of thin films of such substances resulted in high efficiency oxygen reduction, with neat water being the hole scavenger. It was found that the presence of two carbonyl functionalities was the crucial catalytic site towards the reductive transformation of oxygen. The optimum H_2O_2 yield that was acquired was 2.5 μg H_2O_2/mg catalyst/hour.

A melamine foam has been used as a precursor for the preparation of carbon-based supports by an annealing process [51]. During the thermal process, cobalt hydroxide was compounded with the foam structure. After the annealing, Co_3O_4 nanoparticles were supported onto the carbon-based framework. The presence of oxygen vacancies resulted in efficient H_2O_2 generation in the absence of a hole scavenger. The carbon support showed electron-acceptor character, thus catalyzing the oxygen reduction reaction. The optimal H_2O_2 production rate was 3.78 mmol/h/g.

Shiraishi and co-workers [52] synthesized resorcinol-formaldehyde resins as potential metal-free photocatalysts. Such polymeric systems were comprised of benzenoid-quinoid conjugated domains, leading to a broad light absorption up to 700 nm. After 24 h of irradiation, the H_2O_2 maximum amount that was generated was about 3.3 mM. The aforementioned systems were prepared by a base-catalyzed polycondensation process. The same group studied the synthesis of such networks under acidic hydrothermal conditions [53]. After 24 h of irradiation, the H_2O_2 maximum amount that was generated was about 2.7 mM, when using HCl during the synthetic protocol. Similarly, by using oxalic acid for pH adjusting, such resorcinol-formaldehyde networks were doped with poly(3-hexylthiophene) through an autoclave reaction [54]. The highly dispersed conjugated polymer within the network of the crosslinked resin generated charge transfer complexes with the conduction band of the resin. This facilitated efficient transfer of the photogenerated conduction band electrons through the polythiophene backbone. After 6 h of irradiation, the H_2O_2 concentration reached a maximum value of about 2.3 mM.

Analogous polycondensation adducts, such as 4-methoxybenzaldehyde/procyanidin networks, were tested as metal-free photocatalytic systems for H_2O_2 generation [55]. The production rate of hydrogen peroxide reached a value of about 1385 μmol/h/g. The H_2O_2 amount depended strongly on the chosen sacrificial agent as well as the acidity of the aqueous system. Moreover, the integration of carbon dots (CD) within the aforementioned 4-methoxybenzaldehyde/procyanidin network afforded an efficient photocatalytic system towards the H_2O_2 generation in real seawater [56]. CD were shown to act as both the co-catalytic active site as well as the efficient electron acceptor/donor component, improving the catalytic efficiency in the hybrid assembly. The maximum yield of H_2O_2 for the optimal hybrid catalyst was estimated to be 1776 μmol/g/h, in seawater.

Ring-shaped macrocyclic triazine-based systems, bearing either acetylene or diacetylene moieties, have been tested as potential H_2O_2 photocatalysts [57]. The enhancement of photocatalytic activity was attributed to the presence of carbon-carbon triple bonds, which modulate the electronic properties of the frameworks as well as suppress electron-hole recombination.

Similarly, acetylene and diacetylene moieties have been merged with heptazine networks towards the synthesis of ring-shaped semiconductors (Figure 5) [58]. The photocatalytic experiments were conducted in O_2-saturated pure water under visible-light irradiation ($\lambda > 420$ nm). The maximum H_2O_2 production rate was estimated to be about 69 μmol/h. Alternative ring-shaped systems, which construct covalent organic frameworks (COFs), include the ones that are synthesized by coupling reaction between 2,2′-bipyridine-5,5′-diamine and triformylphloroglucinol [59]. The optimized photosynthetic rate of H_2O_2 reached a value of 1042 μM/h under one standard sunlight at 298 K.

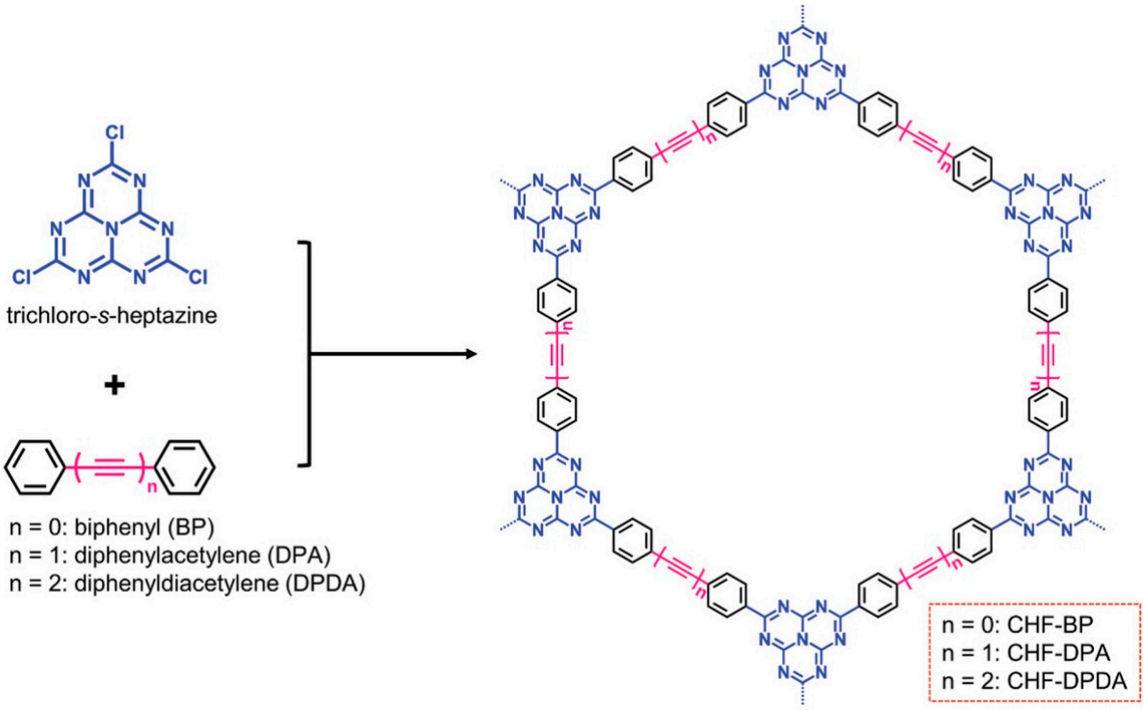

Figure 5. Synthetic protocol for obtaining covalent heptazine frameworks (CHF). Adapted with permission from Ref. [58]. Copyright 2022 Wiley-VCH.

Regarding the chemical architecture of conjugated polymers bearing acetylenic moieties, linear systems of the 3-[(4-ethynylphenyl)ethynyl] pyridine repeating unit have been studied as potential photocatalytic systems [60]. The catalyst was shown to withstand irradiation times up to about 10 h. At longer times, decomposition was found to take place. At 1.5 h irradiation time, the H_2O_2 production rate was about 3 mM.

Kang and co-workers [61] have used an organic semiconductor that was synthesized by a coupling reaction between 9,10-dibromoanthracene and trimethylsilylacetylene. The aforementioned system was studied for the photocatalytic H_2O_2 generation in polar organic media containing trace amounts of water. Under visible light, for an acetonitrile (MeCN) medium containing about 1.5 vol% water, the catalyst was found to generate H_2O_2 with a rate of 3923 μmol/g/h. Furthermore, in a commercially available MeCN with water content below 0.01%, 8.8 mM, H_2O_2 was generated after 12 h reaction, suggesting the water impurity in MeCN was completely removed.

3.7. Graphitic Carbon Nitride (g-C_3N_4) Systems

Among various photocatalysts, polymeric carbon nitride (C_3N_4) is a promising candidate for H_2O_2 production due to its (i) simple synthesis by a calcination process, (ii) structure consisting of earth-abundant carbon and nitrogen, (iii) effective bandgap size for visible light absorption, and (iv) suitable position of the conduction band for the reduction of oxygen in aqueous environment [62–64].

Visible light irradiation of a polymeric semiconductor, graphitic carbon nitride (g-C_3N_4) was found to selectively produce H_2O_2 in the presence of ethanol as a hole scavenger [65]. Electron spin resonance and Raman analysis revealed that the high H_2O_2 selectivity was attributed to the efficient formation of 1,4-endoperoxide species on the g-C_3N_4 lattice. This suppressed the reduction of O_2 to superoxide radical (one-electron mechanism), selectively promoting the reduction of O_2 to H_2O_2 (two-electron mechanism). It is noted that the valence band potential of g-C_3N_4 lies at 1.4 V (versus the NHE), rendering the water oxidation process not favorable thermodynamically. Thus, the modification of the band alignment of the semiconductor seems to be imperative.

Further decoration of carbon nitride surface with electron-deficient aromatic diimide units of pyromellitic type has been shown to shift the potentials of either valence or conduction band of the main semiconductor [66]. After 48 h irradiation, the H_2O_2 production rate was estimated to be 1.65 mM. The proposed mechanism involves two-photon excitation by which two electron/hole pairs were formed (Figure 6). Water molecules are oxidized by the holes, whereas molecular oxygen is reduced by the electrons, thus forming a superoxo radical which subsequently transforms into 1,4-endoperoxide species. Protonation of the latter adduct produces hydrogen peroxide.

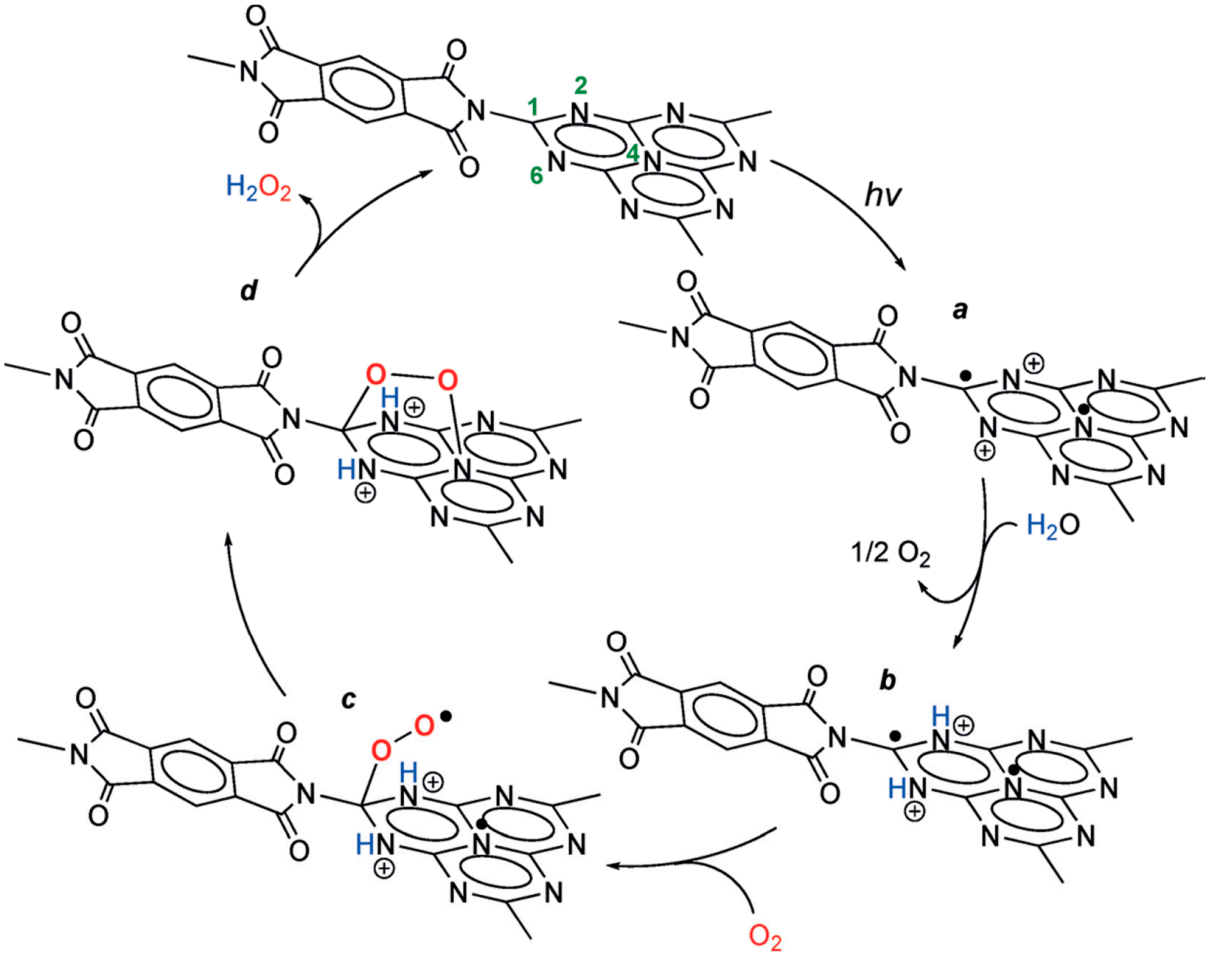

Figure 6. Proposed mechanism for H_2O_2 generation. Adapted with permission from Ref. [66]. Copyright 2014 Wiley-VCH.

In a similar study, biphenyl diimide was used as a co-catalyst for g-C_3N_4 [67]. At 24 h irradiation, the maximum production rate was up to about 0.4 mM. In a subsequent study by the Shiraishi group, pyromellitic diimide-doped C_3N_4 was compounded with boron nitride (BN) and reduced graphene oxide (rGO) flakes [68]. The photoexcited electron was migrated from the g-C_3N_4 conduction band to rGO, leading to the two-electron reduction of O_2 to H_2O_2, whereas the corresponding holes were transferred to BN, leading to the efficient oxidation of water. The integration of dual cocatalysts inhibited the electron–hole recombination process. After 24 h irradiation, the H_2O_2 production rate was estimated to be about 1.2 mM.

Heteroatom-doped C_3N_4 was synthesized through a solid-state thermal polymerization of either melamine or urea in the presence of an appropriate precursor. Kang and co-workers [69] have calcined a mixture of urea and phosphonitrilic chloride in order to acquire P-doped C_3N_4. This heteroatom-doped catalyst showed a very high photocatalytic activity for H_2O_2 generation, with a rate of 1968 μmol/g/h. Similarly, boron-doped C_3N_4

was synthesized through a solid-state thermal polymerization of melamine in the presence of KBH_4 salt [70]. The resulting material demonstrated a leaf-vein-like morphology, which was found to promote the generation of defect sites. The optimal photocatalytic activity for H_2O_2 synthesis reached 300 μM/h. Further derivatization of boron-doped C_3N_4 by zinc polyphthalocyanine took place via copolymerization of 1,2,4,5-tetracyanobenzene and $ZnCl_2$ [71]. The resulting assembly demonstrated an enhanced H_2O_2 production rate of 114 μmol/g/h by using a Z-scheme heterojunction. Ohno and co-workers [72] have developed a method towards the doping of C_3N_4 lattice by single Sb atoms, by solid-state annealing of a melamine-$NaSbF_6$ mixture. The single Sb sites were found to act as an electron acceptor, thus acting as the O_2 photoreduction sites. Simultaneously, the accumulated holes at the N atoms of the C_3N_4 domains adjacent to the Sb sites accelerated the H_2O oxidation kinetics.

In an analogous approach, K/PO_4-doped C_3N_4 was synthesized through a solid-state thermal polymerization of melamine in the presence of K_2HPO_4 salt [73,74]. Thus, the incorporation of both potassium and phosphate species was carried out onto the carbon nitride framework. These incorporated species modified the surface and charge transfer properties, thus enhancing the photoactivities for the generation of H_2O_2. The high photoactivity of doped C_3N_4 towards the production of H_2O_2 (1.7 mM after a 7 h irradiation) was attributed to (1) the enhanced light absorption at UV wavelengths, (2) the increased lifetime of the transient species, (3) the effective interfacial charge transfer to oxygen, and (4) the inhibited decomposition of in situ generated H_2O_2 [73].

Similar hybrid photocatalysts were synthesized through the thermal processing of C_3N_4 precursors with either potassium-based ionic substances [75,76], phosphate salts [77], or thermally annealed MOFs [78]. After visible light irradiation for a 10 h period, the H_2O_2 concentration was estimated to be 5 mM, which was more than five times higher than the one that was achieved by calcined neat urea [77].

Alternatively, an ionothermal method was applied between C_3N_4 and a mixture of alkali chlorides (Figure 7) [79]. It was suggested that either potassium or sodium cations were positioned at specific sites of the C_3N_4 lattice, containing nitrogen/oxygen-based anionic species. The synergistic effect of doping and defect engineering resulted in the enhancement of photocatalytic performance with an H_2O_2 production rate of 10.2 mmol/h/g, a value which was about 90 times higher than the one of neat C_3N_4.

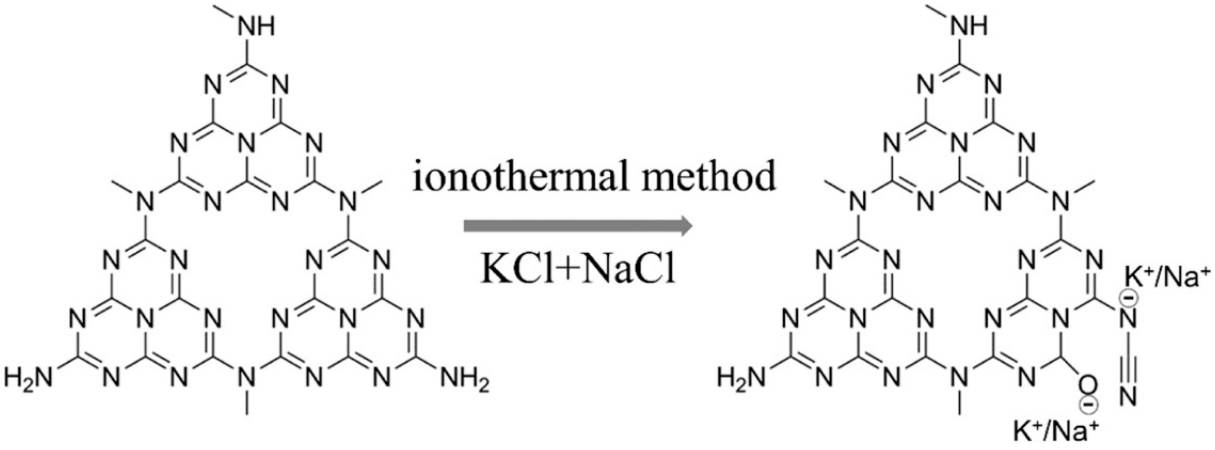

Figure 7. Introduction of alkali metal dopants onto a C_3N_4 lattice. Adapted with permission from Ref. [79]. Copyright 2020 ACS.

In an analogous work, a $Cu_2(OH)PO_4$/g-C_3N_4 hybrid photocatalyst was synthesized by compounding within an autoclave reactor [80]. The aforementioned hybrid exhibited a full-spectrum-response from UV to the near IR region and the excitation mechanism involved a Z-scheme module. A $Cu_2(OH)PO_4$ ionic substance was suggested to form photogenerated electrons, which were recombined with the holes of a g-C_3N_4 valence

band. Simultaneously, $Cu_2(OH)PO_4$ may adsorb O_2 molecules, which is significantly important in the photocatalytic process. The $Cu_2(OH)PO_4$/g-C_3N_4 heterojunction catalyst with a $Cu_2(OH)PO_4$ of 20 wt % showed an optimal H_2O_2 concentration of 7.2 mM, over 13 and 31.3 times higher than the ones of neat g-C_3N_4 and $Cu_2(OH)PO_4$, respectively. The photocatalytic generation of H_2O_2 under a Z-scheme mechanism was assessed by using $Bi_4O_5Br_2$/g-C3N4 hybrids [81]. The optimal H_2O_2 production rate was 124 μM/h. The electrons and holes of the hybrid were mainly derived from the g-C_3N_4 conduction band and the $Bi_4O_5Br_2$ valence band, respectively.

Metal phosphides have been applied as functional cocatalysts for C_3N_4-based systems. Specifically, cobalt phosphide (CoP) nanoparticles were embedded within the network of carbon nitride [82]. The optimal catalyst with 1.76 wt% CoP content demonstrated enhanced photocatalytic efficiency with an H_2O_2 production rate of 140 μM after 2 h irradiation time, which was about 4.6 and 23.3 times higher than the ones of neat g-C_3N_4 and CoP, respectively. In an analogous study, carbon nitride and WO_3 nanoparticles have been compounded through a solid-state calcination of dicyandiamide and ammonium paratungstate mixture [83]. The authors proposed oxygen-enriched carbon nitride models, which were proven to generate 1,4-endoperoxide species more efficiently, rather than superoxide radicals, through theoretical calculations and experimental investigation. Under an oxygen-saturated atmosphere and the presence of isopropanol as a hole scavenger, the highest yield that was achieved by the hybrid calcined at 500 °C reached 730 μmol after 5 h. Chen and co-workers [84] fabricated graphitic carbon nitride that was enriched with cyano groups, via solid-state thermal annealing of NaCl-dicyandiamide mixtures. The cyano groups were suggested to adjust the band structure of C_3N_4 as well as act as oxygen adsorption sites. The resulting photocatalysts exhibited superior activity towards the H_2O_2 generation. Irradiation in the visible region afforded a rate of 7 mM/h, whereas the corresponding rate under simulated sun conditions was 16 mM/h.

The covalent anchoring of aromatic substances onto the C_3N_4 surface has been used in order to inhibit carrier recombination phenomena. Kim and co-workers [85] have attached anthraquinone molecules onto the carbon nitride surface. The suggested mechanism involves the hydrogenation reaction of anthraquinone moieties to AQH_2 and the subsequent generation of H_2O_2 by oxygen reduction, mediated through the dehydrogenation reaction of AQH_2 intermediate substance. A H_2O_2 production rate of 361 μmol/g/h at 380 nm excitation wavelength was achieved using the hybrid material in the presence of an organic electron donor (2-propanol).

Regarding the hybridization of carbon nitride with graphitic allotropes, Zhao and co-workers [86] have applied a protocol, leading to the covalent attachment of carbon nanotubes (CNTs) onto the carbon nitride surface, by an amidation reaction. The presence of the conductive co-catalyst was found to enhance the reducing ability of photoexcited semiconductor. The g-C_3N_4-CNTs hybrid exhibited remarkable catalytic performance for photocatalytic H_2O_2 generation in the presence of formic acid as a hole scavenger (32.6 μmol/h).

In an interesting work, Kang and co-workers [87] have studied the synergistic effect of C_3N_4, a conductive needle coke and a green microalga (*Chlorella vulgaris*) towards the photocatalytic generation of H_2O_2. In this three-component system, the needle coke served as cocatalyst to enhance the separation of photoinduced electron–hole pairs of g-C_3N_4, which provides oxidation sites for partial H_2O_2 evolution. The living *C. vulgaris* participated to the H_2O_2 evolution through an oxygen reduction process. The optimal three-component photocatalyst exhibited a H_2O_2 production rate of 0.98 μmol/h.

By using the aforementioned principle of the dual cocatalyst, Li et al. [88] have compounded C_3N_4 with organic small molecules and N,S-doped carbon dots. The organic substance was a carbazole derivative which acted as the active site of oxygen reduction reaction (ORR), and carbon dots were suggested to participate as the active site of water oxidation reaction (WOR) [89]. The three-component catalyst exhibited a remarkable H_2O_2 production rate of 2203 μmol/h/g.

4. State-of-the-Art and Future Prospects

In Table 1, we selected the works which have exhibited the higher H_2O_2 production rates. As clearly shown, the most efficient photocatalytic systems involve the ones that are related to either porous carbon nitride assemblies, metal organic frameworks, or carbon-based conjugated semiconducting nanostructures. However, the most important aspects seem to be tailored doping with heterostructures as well as the generation of functional defect sites. These may enhance the selectivity of the two-electron oxygen reduction reaction and suppress the electron-hole recombination process. Furthermore, the dopants act as oxygen adsorption sites, thus enhancing the photocatalytic activity. This puts into discussion the very important aspect of high surface area assemblies. Various protocols should be developed, based on sacrificial template approaches, in order to acquire doped semiconductors with available catalytic sites. The combination of chemical modification and porosity enhancement may pave the way towards the development of highly efficient photocatalytic systems in aqueous environments.

Table 1. Selected photocatalytic systems for H_2O_2 production (decreasing yield order).

Main Semiconductor	Co-Catalyst/Dopant	Band Gap (eV)	H_2O_2 Yield (μmol/g/h)	Reference (Year)
Cyano-C_3N_4	Na^+	2.53	16,000	[84] (2021)
NH_2-UiO-66(Zr)@OPA MOF	Ti^{4+}	nd	13,580	[49] (2020)
C_3N_4	K^+/Na^+	2.63	10,200	[79] (2020)
C_3N_4	K^+	2.75	10,000	[76] (2022)
C_3N_4	ZnO	2.83	4000	[78] (2021)
Anthracene/ acetylene-based semiconductor	-	2.89	3923	[61] (2022)
Carbon support	Co_3O_4	1.84–1.97	3785	[51] (2019)
TiO_2 nanotubes	Carbon dots	2.98	3420	[20] (2019)
C_3N_4	-	2.68	3103	[90] (2019)
C_3N_4	WO_3	2.60	2920	[83] (2018)
$NiTiO_3$	-	3.00	2500	[37] (2018)
3-[(4-ethynylphenyl) ethynyl]pyridine polymer	-	2.34	2267	[60] (2021)
C_3N_4	N,S-doped carbon dots plus carbazole derivative	2.58	2203	[88] (2021)
C_3N_4	$(COOH)_2$	2.42	2008	[91] (2021)
C_3N_4	P	2.58	1968	[69] (2020)
C_3N_4	Ti_3C_2	2.60	1847	[92] (2021)
4-methoxybenzaldehyde/ procyanidin network	Carbon dots	1.94	1776	[56] (2021)

nd: not determined.

Concerning the integration of such hybrids in industrial scale facilities, some promising results have been achieved, yet additional work has to be performed. The main parameter which needs to be addressed is the cost of the process, including the development of facilities utilizing the solar light as an excitation source. A significant advance in the field could be achieved by catalytic systems which are synthesized by one-pot processes. This would significantly decrease the cost of the whole process in the synthetic part. As shown in Table 1, C_3N_4-based nanostructures are considered as potentially efficient photocatalytic systems for H_2O_2 evolution. This is greatly supported by the fact that such systems are derived by one-step annealing processes. Issues that are related with electron-hole recombination phenomena, could be resolved by developing functional Z-scheme binary systems acquiring spatial separation of the carriers. Our strong belief is that the industrial-scale H_2O_2 evolution and subsequent utilization is much closer to achievement, when compared with the state-of-the-art methods that were acquired a couple of years ago. The H_2O_2 yield as well as the response of the catalysts to visible light have been widely enhanced in the recent years. Further research should be focused on the development of photocatalytic systems with high recyclability.

Author Contributions: Writing—original draft preparation, N.K. and D.T.; writing—review and editing, N.K. and D.T. All authors have read and agreed to the published version of the manuscript.

Funding: This research received no external funding.

Institutional Review Board Statement: Not applicable.

Informed Consent Statement: Not applicable.

Data Availability Statement: Not applicable.

Conflicts of Interest: The authors declare no conflict of interest.

Abbreviations

AQ	Anthraquinone
Tris	tris(hydroxymethyl) aminomethane
TNT	TiO_2 nanotubes
CA	Citric acid
CD	Carbon dots
NP	Nanoparticles
rGO	Reduced graphene oxide
MOF	Metal-organic framework
OPA	Organophosphonic acid
BP	Biphenyl
DPA	Diphenylacetylene
DPDA	Diphenyldiacetylene
CHF	Covalent heptazine framework
COF	Covalent organic framework
NHE	Normal hydrogen electrode
BN	Boron nitride
CNT	Carbon nanotubes
ORR	Oxygen reduction reaction
WOR	Water oxidation reaction

References

1. Nosaka, Y.; Nosaka, A.Y. Generation and detection of reactive oxygen species in photocatalysis. *Chem. Rev.* **2017**, *117*, 11302–11336. [CrossRef] [PubMed]
2. Chatterjee, D.; Dasgupta, S. Visible light induced photocatalytic degradation of organic pollutants. *J. Photochem. Photobiol. C Photochem. Rev.* **2005**, *6*, 186–205. [CrossRef]
3. Tu, W.; Zhou, Y.; Zou, Z. Photocatalytic conversion of CO_2 into renewable hydrocarbon fuels: State-of-the-art accomplishment, challenges, and prospects. *Adv. Mater.* **2014**, *26*, 4607–4626. [PubMed]
4. Lianos, P. Review of recent trends in photoelectrocatalytic conversion of solar energy to electricity and hydrogen. *Appl. Catal. B: Environ.* **2017**, *210*, 235–254.
5. Hou, H.; Zeng, X.; Zhang, X. Production of hydrogen peroxide by photocatalytic processes. *Angew. Chem. Int. Ed.* **2020**, *59*, 17356–17376. [CrossRef]
6. Prat, C.; Vicente, M.; Esplugas, S. Treatment of bleaching waters in the paper industry by hydrogen peroxide and ultraviolet radiation. *Water Res.* **1988**, *22*, 663–668. [CrossRef]
7. Ksibi, M. Chemical oxidation with hydrogen peroxide for domestic wastewater treatment. *Chem. Engin. J.* **2006**, *119*, 161–165. [CrossRef]
8. Nishimi, T.; Kamachi, T.; Kato, K.; Kato, T.; Yoshizawa, K. Mechanistic study on the production of hydrogen peroxide in the anthraquinone process. *Eur. J. Org. Chem.* **2011**, *2011*, 4113–4120. [CrossRef]
9. Liu, T.; Pan, Z.; Kato, K.; Wu, B.; Yamakata, A.; Katayama, K.; Chen, B.; Chu, C.; Domen, K. Overall photosynthesis of H_2O_2 by an inorganic semiconductor. *Nat. Commun.* **2022**, *13*, 1034. [CrossRef]
10. Zhang, F.; Wang, X.; Liu, H.; Liu, C.; Wan, Y.; Long, Y.; Cai, Z. Recent advances and applications of semiconduction photocatalytic technology. *Appl. Sci.* **2019**, *9*, 2489.
11. Harbour, J.R.; Tromp, J.; Hair, M.L. Photogeneration of hydrogen peroxide in aqueous TiO_2 dispersions. *Can. J. Chem.* **1985**, *63*, 204–208. [CrossRef]
12. Cai, R.; Kubota, Y.; Fujishima, A. Effect of copper ions on the formation of hydrogen peroxide from photocatalytic titanium dioxide particles. *J. Catal.* **2003**, *219*, 214–218. [CrossRef]
13. Diesen, V.; Jonsson, M. Formation of H_2O_2 in TiO_2 photocatalysis of oxygenated and deoxygenated aqueous systems: A probe for photocatalytically produced hydroxyl radicals. *J. Phys. Chem. C* **2014**, *118*, 10083–10087. [CrossRef]

14. Muraki, H.; Saji, T.; Fujihira, M.; Aouagui, S. Photocatalytic oxidation of water to hydrogen peroxide by irradiation of aqueous suspensions of TiO_2. *J. Electroanal. Chem.* **1984**, *169*, 319–323. [CrossRef]
15. Cormann, C.; Bahnemann, D.W.; Hoffmann, M.R. Photocatalytic production of H_2O_2 and organic peroxides in aqueous suspensions of TiO_2, ZnO and desert sand. *Environ. Sci. Technol.* **1988**, *22*, 798–806. [CrossRef]
16. Goto, H.; Hanada, Y.; Ohno, T.; Matsumura, M. Quantitative analysis of superoxide ion and hydrogen peroxide produced from molecular oxygen in photoirradiated TiO_2 particles. *J. Catal.* **2004**, *225*, 223–229. [CrossRef]
17. Mrowetz, M.; Selli, E. Photocatalytic degradation of formic and benzoic acids and hydrogen peroxide evolution in TiO_2 and ZnO water suspensions. *J. Photochem. Photobiol. A Chem.* **2006**, *180*, 15–22. [CrossRef]
18. Shiraishi, Y.; Kanazawa, S.; Tsukamoto, D.; Shiro, A.; Sugano, Y.; Hirai, T. Selective hydrogen peroxide formation by titanium dioxide photocatalysis with benzylic alcohols and molecular oxygen in water. *ACS Catal.* **2013**, *3*, 2222–2227. [CrossRef]
19. Hirakawa, T.; Nosaka, Y. Selective production of superoxide ions and hydrogen peroxide over nitrogen- and sulfur-doped TiO_2 photocatalysts with visible light in aqueous suspension systems. *J. Phys. Chem. C* **2008**, *112*, 15818–15823. [CrossRef]
20. Ma, R.; Wang, L.; Liu, Z.; Xing, M.; Zhu, L.; Meng, X.; Xiao, F.-S. Solid acids accelerate the photocatalytic hydrogen peroxide synthesis over a hybrid catalyst of titania nanotube with carbon dot. *Appl. Catal. B Environ.* **2019**, *244*, 594–603.
21. Zheng, L.; Zhang, J.; Hu, Y.H.; Long, M. Enhanced photocatalytic production of H_2O_2 by Nafion coatings on S,N-codoped graphene-quantum-dots-modified TiO_2. *J. Phys. Chem. C* **2019**, *123*, 13693–13701. [CrossRef]
22. Lee, T.; Bui, H.T.; Yoo, J.; Ra, M.; Han, S.H.; Kim, W.; Kwon, W. Formation of TiO_2@carbon core/shell nanocomposites from a single molecular layer of aromatic compounds for photocatalytic hydrogen peroxide generation. *ACS Appl. Mater. Interf.* **2019**, *11*, 41196–41203. [CrossRef] [PubMed]
23. Wu, X.; Zhang, X.; Zhao, S.; Gong, Y.; Lin, S.; Zhao, X. Highly-efficient photocatalytic hydrogen peroxide production over polyoxometalates covalently immobilized onto titanium dioxide. *Appl. Catal. A* **2020**, *591*, 117271. [CrossRef]
24. Maurino, V.; Minero, C.; Mariella, G.; Pelizzetti, E. Sustained production of H_2O_2 on irradiated TiO_2-fluoride systems. *Chem. Commun.* **2005**, 2627–2629. [CrossRef]
25. Teranishi, M.; Naya, S.; Tada, H. In situ liquid phase synthesis of hydrogen peroxide from molecular oxygen using gold nanoparticle-loaded titanium(IV) dioxide photocatalyst. *J. Amer. Chem. Soc.* **2010**, *132*, 7850–7851. [CrossRef]
26. Teranishi, M.; Naya, S.; Tada, H. Temperature- and pH-dependence of hydrogen peroxide formation from molecular oxygen by gold nanoparticle-loaded titanium(IV) oxide photocatalyst. *J. Phys. Chem. C* **2016**, *120*, 1083–1088. [CrossRef]
27. Tsukamoto, D.; Shiro, A.; Shiraishi, Y.; Ichikawa, S.; Tanaka, S.; Hirai, T. Photocatalytic H_2O_2 production from ethanol/O_2 system using TiO_2 loaded with Au−Ag bimetallic alloy nanoparticles. *ACS Catal.* **2012**, *2*, 599–603. [CrossRef]
28. Kaynan, N.; Berke, B.A.; Hazut, O.; Yerushalmi, R. Sustainable photocatalytic production of hydrogen peroxide from water and molecular oxygen. *J. Mater. Chem. A* **2014**, *2*, 13822–13826. [CrossRef]
29. Kim, K.; Park, J.; Kim, H.; Jung, G.Y.; Kim, M.G. Solid-phase photocatalysts: Physical vapor deposition of Au nanoislands on porous TiO_2 films for millimolar H_2O_2 production within a few minutes. *ACS Catal.* **2019**, *9*, 9206–9211. [CrossRef]
30. Zuo, G.; Li, B.; Guo, Z.; Wang, L.; Yang, F.; Hou, W.; Zhang, S.; Zong, P.; Liu, S.; Meng, X.; et al. Efficient Photocatalytic Hydrogen Peroxide production over TiO_2 Passivated by SnO_2. *Catalysts* **2019**, *9*, 623. [CrossRef]
31. Awa, K.; Naya, S.; Fujishima, M.; Tada, H. A Three-Component Plasmonic Photocatalyst Consisting of Gold Nanoparticle and TiO_2−SnO_2 Nanohybrid with Heteroepitaxial Junction: Hydrogen Peroxide Synthesis. *J. Phys. Chem. C* **2020**, *124*, 7797–7802. [CrossRef]
32. Hoffman, A.J.; Carraway, E.R.; Hoffmann, M.R. Photocatalytic Production of H_20_2 and Organic Peroxides on Quantum-Sized Semiconductor Colloids. *Environ. Sel. Technol.* **1994**, *28*, 776–785. [CrossRef]
33. Liu, Y.; Han, J.; Qiu, W.; Gao, W. Hydrogen peroxide generation and photocatalytic degradation of estrone by microstructural controlled ZnO nanorod arrays. *Appl. Surf. Sci.* **2012**, *263*, 389–396. [CrossRef]
34. Hirakawa, H.; Shiota, S.; Shiraishi, Y.; Sakamoto, H.; Ichikawa, S.; Hirai, T. Au Nanoparticles Supported on $BiVO_4$: Effective Inorganic Photocatalysts for H_2O_2 Production from Water and O_2 under Visible Light. *ACS Catal.* **2016**, *8*, 4976–4982. [CrossRef]
35. Teranishi, M.; Kunimoto, T.; Naya, S.; Kobayashi, H.; Tada, H. Visible-Light-Driven Hydrogen Peroxide Synthesis by a Hybrid Photocatalyst Consisting of Bismuth Vanadate and Bis(hexafluoroacetylacetonato)copper(II) Complex. *J. Phys. Chem. C* **2020**, *124*, 3715–3721. [CrossRef]
36. Dhabarde, N.; Carrillo-Ceja, O.; Tian, S.; Xiong, G.; Raja, K.; Subramanian, V.R. Bismuth Vanadate Encapsulated with Reduced Graphene Oxide: A Nanocomposite for Optimized Photocatalytic Hydrogen Peroxide Generation. *J. Phys. Chem. C* **2021**, *125*, 23669–23679. [CrossRef]
37. Baran, T.; Wojtyła, S.; Vertova, A.; Minguzzi, A.; Rondinini, S. Photoelectrochemical and photocatalytic systems based on titanates for hydrogen peroxide formation. *J. Electroanal. Chem.* **2018**, *808*, 395–402. [CrossRef]
38. Zhang, Y.; Park, S.J. Formation of hollow MoO_3/SnS_2 heterostructured nanotubes for efficient light-driven hydrogen peroxide production. *J. Mater. Chem. A* **2018**, *6*, 20304–20312. [CrossRef]
39. Thakur, S.; Kshetri, T.; Kim, N.H.; Lee, J.H. Sunlight-driven sustainable production of hydrogen peroxide using a CdS–graphene hybrid photocatalyst. *J. Catal.* **2017**, *345*, 78–86. [CrossRef]
40. Zhang, H.; Bai, X. Photocatalytic production of hydrogen peroxide over Z-scheme Mn_3O_4/ Co_9S_8 with p-n heterostructure. *Appl. Catal. B Environ.* **2021**, *298*, 120516. [CrossRef]

41. Tian, Z.; Han, C.; Zhao, Y.; Dai, W.; Lian, X.; Wang, Y.; Zheng, Y.; Shi, Y.; Pan, X.; Huang, Z.; et al. Efficient photocatalytic hydrogen peroxide generation coupled with selective benzylamine oxidation over defective ZrS_3 nanobelts. *Nat. Commun.* **2021**, *12*, 2039. [CrossRef] [PubMed]
42. Li, Y.; Zhao, Y.; Nie, H.; Wei, K.; Cao, J.; Huang, H.; Shao, M.; Liu, Y.; Kang, Z. Interface photo-charge kinetics regulation by carbon dots for efficient hydrogen peroxide production. *J. Mater. Chem. A* **2021**, *9*, 515. [CrossRef]
43. Chen, X.; Kondo, Y.; Kuwahara, Y.; Mori, K.; Louis, C.; Yamashita, H. Metal–organic framework-based nanomaterials for photocatalytic hydrogen peroxide production. *Phys. Chem. Chem. Phys.* **2020**, *22*, 14404. [CrossRef] [PubMed]
44. Isaka, Y.; Kondo, Y.; Kawase, Y.; Kuwahara, Y.; Mori, K.; Yamashita, H. Photocatalytic production of hydrogen peroxide through selective two-electron reduction of dioxygen utilizing amine-functionalized MIL-125 deposited with nickel oxide nanoparticles. *Chem. Commun.* **2018**, *54*, 9270. [CrossRef]
45. Liu, C.; Bao, T.; Yuan, L.; Zhang, C.; Wang, J.; Wan, J.; Yu, C. Semiconducting MOF@ZnS Heterostructures for Photocatalytic Hydrogen Peroxide Production: Heterojunction Coverage Matters. *Adv. Funct. Mater.* **2022**, *32*, 2111404. [CrossRef]
46. Isaka, Y.; Kawase, Y.; Kuwahara, Y.; Mori, K.; Yamashita, H. Two-Phase System Utilizing Hydrophobic Metal-Organic Frameworks for Photocatalytic Synthesis of Hydrogen Peroxide. *Angew. Chem. Int. Ed.* **2019**, *58*, 5402–5406. [CrossRef]
47. Kawase, Y.; Isaka, Y.; Kuwahara, Y.; Mori, K.; Yamashita, H. Ti cluster-alkylated hydrophobic MOFs for photocatalytic production of hydrogen peroxide in two-phase systems. *Chem. Commun.* **2019**, *55*, 6743. [CrossRef]
48. Chen, X.; Kuwahara, Y.; Mori, K.; Louis, C.; Yamashita, H. Introduction of a secondary ligand into titanium-based metal–organic frameworks for visible-light-driven photocatalytic hydrogen peroxide production from dioxygen reduction. *J. Mater. Chem. A* **2021**, *9*, 2815–2821. [CrossRef]
49. Chen, X.; Kuwahara, Y.; Mori, K.; Louis, C.; Yamashita, H. Hydrophobic Titanium Doped Zirconium-based Metal Organic Framework for Photocatalytic Hydrogen Peroxide Production in Two-phase System. *J. Mater. Chem. A* **2020**, *8*, 1904–1910. [CrossRef]
50. Wecławski, M.K.; Jakesova, M.; Charyton, M.; Demitri, N.; Koszarna, B.; Oppelt, K.; Sariciftci, S.; Gryko, D.T.; Głowacki, E.D. Biscoumarin-containing acenes as stable organic semiconductors for photocatalytic oxygen reduction to hydrogen peroxide. *J. Mater. Chem. A* **2017**, *5*, 20780–20788. [CrossRef]
51. Zhu, C.; Zhu, M.; Sun, Y.; Zhou, Y.; Gao, J.; Huang, H.; Liu, Y.; Kang, Z. Carbon-Supported Oxygen Vacancy-Rich Co_3O_4 for Robust Photocatalytic H_2O_2 Production via Coupled Water Oxidation and Oxygen Reduction Reaction. *ACS Appl. Energy Mater.* **2019**, *2*, 8737–8746. [CrossRef]
52. Shiraishi, Y.; Takii, T.; Hagi, T.; Mori, S.; Kofuji, Y.; Kitagawa, Y.; Tanaka, S.; Ichikawa, S.; Hirai, T. Resorcinol–formaldehyde resins as metal-free semiconductor photocatalysts for solar-to hydrogen peroxide energy conversion. *Nat. Mater.* **2019**, *18*, 985–993. [CrossRef] [PubMed]
53. Shiraishi, Y.; Hagi, T.; Matsumoto, M.; Tanaka, S.; Ichikawa, S.; Hirai, T. Solar-to-hydrogen peroxide energy conversion on resorcinol–formaldehyde resin photocatalysts prepared by acid-catalysed polycondensation. *Commun. Chem.* **2020**, *3*, 169. [CrossRef]
54. Shiraishi, Y.; Matsumoto, M.; Ichikawa, S.; Tanaka, S.; Hirai, T. Polythiophene-Doped Resorcinol−Formaldehyde Resin Photocatalysts for Solar-to-Hydrogen Peroxide Energy Conversion. *J. Amer. Chem. Soc.* **2021**, *143*, 12590–12599. [CrossRef] [PubMed]
55. Wu, Q.; Liu, Y.; Cao, J.; Sun, Y.; Liao, F.; Liu, Y.; Huang, H.; Shao, M.; Kang, Z. A function-switchable metal-free photocatalyst for the efficient and selective production of hydrogen and hydrogen peroxide. *J. Mater. Chem. A* **2020**, *8*, 11773–11780. [CrossRef]
56. Wu, Q.; Cao, J.; Wang, X.; Liu, Y.; Zhao, Y.; Wang, H.; Liu, Y.; Huang, H.; Liao, F.; Shao, M.; et al. A metal-free photocatalyst for highly efficient hydrogen peroxide photoproduction in real seawater. *Nat. Commun.* **2021**, *12*, 483. [CrossRef]
57. Chen, L.; Wang, L.; Wan, Y.; Zhang, Y.; Qi, Z.; Wu, X.; Xu, H. Acetylene and Diacetylene Functionalized Covalent Triazine Frameworks as Metal-Free Photocatalysts for Hydrogen Peroxide Production: A New Two-Electron Water Oxidation Pathway. *Adv. Mater.* **2020**, *32*, 1904433. [CrossRef]
58. Cheng, H.; Lv, H.; Cheng, J.; Wang, L.; Wu, X.; Xu, H. Rational Design of Covalent Heptazine Frameworks with Spatially Separated Redox Centers for High-Efficiency Photocatalytic Hydrogen Peroxide Production. *Adv. Mater.* **2022**, *34*, 2107480. [CrossRef]
59. Kou, M.; Wang, Y.; Xu, Y.; Ye, L.; Huang, Y.; Jia, B.; Li, H.; Ren, J.; Deng, Y.; Chen, J.; et al. Molecularly Engineered Covalent Organic Frameworks for Hydrogen Peroxide Photosynthesis. *Angew. Chem. Int. Ed.* **2022**, *16*, e202200413.
60. Liu, L.; Gao, M.Y.; Yang, H.; Wang, X.; Li, X.; Cooper, A.I. Linear Conjugated Polymers for Solar-Driven Hydrogen Peroxide Production: The Importance of Catalyst Stability. *J. Amer. Chem. Soc.* **2021**, *143*, 19287–19293. [CrossRef]
61. Wu, Z.; Wang, X.; Li, Y.; Zhao, H.; Wang, J.; Huang, H.; Liu, Y.; Kang, Z. Converting water impurity in organic solvent into hydrogen and hydrogen peroxide by organic semiconductor photocatalyst. *Appl. Catal. B Environ.* **2022**, *305*, 121047. [CrossRef]
62. Torres-Pinto, A.; Sampaio, M.J.; Silva, C.G.; Faria, J.L.; Silva, A.M.T. Recent Strategies for Hydrogen Peroxide Production by Metal-Free Carbon Nitride Photocatalysts. *Catalysts* **2019**, *9*, 990. [CrossRef]
63. Haider, Z.; Cho, H.; Moon, G.; Kim, H. Minireview: Selective production of hydrogen peroxide as a clean oxidant over structurally tailored carbon nitride photocatalysts. *Catal. Today* **2019**, *335*, 55–64. [CrossRef]
64. Yan, B.; Chen, Z.; Xu, Y. Amorphous and Crystalline 2D Polymeric Carbon Nitride Nanosheets for Photocatalytic Hydrogen/Oxygen Evolution and Hydrogen Peroxide Production. *Chem. Asian J.* **2020**, *15*, 2329–2340. [CrossRef]

65. Shiraishi, Y.; Kanazawa, S.; Sugano, Y.; Tsukamoto, D.; Sakamoto, H.; Ichikawa, S.; Hirai, T. Highly Selective Production of Hydrogen Peroxide on Graphitic Carbon Nitride (g-C_3N_4) Photocatalyst Activated by Visible Light. *ACS Catal.* **2014**, *4*, 774–780. [CrossRef]
66. Shiraishi, Y.; Kanazawa, S.; Kofuji, Y.; Sakamoto, H.; Ichikawa, S.; Tanaka, S.; Hirai, T. Sunlight-Driven Hydrogen Peroxide Production from Water and Molecular Oxygen by Metal-Free Photocatalysts. *Angew. Chem. Int. Ed.* **2014**, *126*, 13672–13677. [CrossRef]
67. Kofuji, Y.; Ohkita, S.; Shiraishi, Y.; Sakamoto, H.; Tanaka, S.; Ichikawa, S.; Hirai, T. Graphitic Carbon Nitride Doped with Biphenyl Diimide: Efficient Photocatalyst for Hydrogen Peroxide Production from Water and Molecular Oxygen by Sunlight. *ACS Catal.* **2016**, *6*, 7021–7029. [CrossRef]
68. Kofuji, Y.; Isobe, Y.; Shiraishi, Y.; Sakamoto, H.; Ichikawa, S.; Tanaka, S.; Hirai, T. Hydrogen Peroxide Production on Carbon Nitride–Boron Nitride– Reduced Graphene Oxide Hybrid Photocatalyst under Visible Light. *ChemCatChem* **2018**, *10*, 2070–2077. [CrossRef]
69. Cao, J.; Wang, H.; Zhao, Y.; Liu, Y.; Wu, Q.; Huang, H.; Shao, M.; Liu, Y.; Kang, Z. Phosphorus-doped porous carbon nitride for efficient sole production of hydrogen peroxide via photocatalytic water splitting with a two-channel pathway. *J. Mater. Chem. A* **2020**, *8*, 3701–3707. [CrossRef]
70. Feng, C.; Tang, L.; Deng, Y.; Wang, J.; Luo, J.; Liu, Y.; Ouyang, X.; Yang, H.; Yu, J.; Wang, J. Synthesis of Leaf-Vein-Like g-C_3N_4 with Tunable Band Structures and Charge Transfer Properties for Selective Photocatalytic H_2O_2 Evolution. *Adv. Funct. Mater.* **2020**, *30*, 2001922. [CrossRef]
71. Ye, Y.X.; Pan, J.; Xie, F.; Gong, L.; Huang, S.; Ke, Z.; Zhu, F.; Xu, J.; Ouyang, G. Highly efficient photosynthesis of hydrogen peroxide in ambient conditions. *Proc. Nat. Acad. Sci. USA* **2021**, *118*, e2103964118. [CrossRef] [PubMed]
72. Teng, Z.; Zhang, Q.; Yang, H.; Kato, K.; Yang, W.; Lu, Y.R.; Liu, S.; Wang, C.; Yamakata, A.; Su, C.; et al. Atomically dispersed antimony on carbon nitride for the artificial photosynthesis of hydrogen peroxide. *Nat. Catal.* **2021**, *4*, 374–384. [CrossRef]
73. Moon, G.; Fujitsuka, M.; Kim, S.; Majima, T.; Wang, X.; Choi, W. Eco-Friendly Photochemical Production of H_2O_2 through O_2 Reduction over Carbon Nitride Frameworks Incorporated with Multiple Heteroelements. *ACS Catal.* **2017**, *7*, 2886–2895. [CrossRef]
74. Fattahimoghaddam, H.; Mahvelati-Shamsabadi, T.; Jeong, C.S.; Lee, B.K. Coral-like potassium and phosphorous doped graphitic carbon nitride structures with enhanced charge and mass transfer dynamics toward photocatalytic hydrogen peroxide production and microbial disinfection. *J. Coll. Interf. Sci.* **2022**, *617*, 326–340. [CrossRef]
75. Tian, J.; Wang, D.; Li, S.; Pei, Y.; Qiao, M.; Li, Z.; Zhang, J.; Zong, B. KOH-Assisted Band Engineering of Polymeric Carbon Nitride for Visible Light Photocatalytic Oxygen Reduction to Hydrogen Peroxide. *ACS Sustain. Chem. Eng.* **2020**, *8*, 594–603. [CrossRef]
76. Xu, Z.; Li, Y.; Cao, Y.; Du, R.; Bao, Z.; Zhang, S.; Shao, F.; Ji, W.; Yang, J.; Zhuang, G.; et al. Trace water triggers high-efficiency photocatalytic hydrogen peroxide production. *J. Energy Chem.* **2022**, *64*, 47–54. [CrossRef]
77. Tian, J.; Wu, T.; Wang, D.; Pei, Y.; Qiao, M.; Zong, B. One-pot synthesis of potassium and phosphorus-doped carbon nitride catalyst derived from urea for highly efficient visible light-driven hydrogen peroxide production. *Catal. Today* **2019**, *330*, 171–178. [CrossRef]
78. Liu, B.; Bie, C.; Zhang, Y.; Wang, L.; Li, Y.; Yu, J. Hierarchically Porous ZnO/g-C_3N_4 S-Scheme Heterojunction Photocatalyst for Efficient H_2O_2 Production. *Langmuir* **2021**, *37*, 14114–14124. [CrossRef]
79. Wu, S.; Yu, H.; Chen, S.; Qua, X. Enhanced Photocatalytic H_2O_2 Production over Carbon Nitride by Doping and Defect Engineering. *ACS Catal.* **2020**, *10*, 14380–14389. [CrossRef]
80. Wang, X.; Han, Z.; Yu, L.; Liu, C.; Liu, Y.; Wu, G. Synthesis of Full-Spectrum-Response $Cu_2(OH)PO_4$/g-C_3N_4 Photocatalyst with Outstanding Photocatalytic H_2O_2 Production Performance via a "Two Channel Route". *ACS Sustain. Chem. Eng.* **2018**, *6*, 14542–14553. [CrossRef]
81. Zhao, X.; You, Y.; Huang, S.; Wu, Y.; Ma, Y.; Zhang, G.; Zhang, Z. Z-scheme photocatalytic production of hydrogen peroxide over $Bi_4O_5Br_2$/g-C_3N_4 heterostructure under visible light. *Appl. Catal. B Environ.* **2020**, *278*, 119251. [CrossRef]
82. Peng, Y.; Wang, L.; Liu, Y.; Chen, H.; Lei, J.; Zhang, J. Visible-light-driven photocatalytic H_2O_2 production on g-C_3N_4 loaded with CoP as a noble metal free cocatalyst. *Eur. J. Inorg. Chem.* **2017**, *40*, 4797–4802. [CrossRef]
83. Wei, Z.; Liu, M.; Zhang, Z.; Yao, W.; Tan, H.; Zhu, Y. Efficient visible-light-driven selective oxygen reduction to hydrogen peroxide by oxygen-enriched graphitic carbon nitride polymers. *Energy Environ. Sci.* **2018**, *11*, 2581–2589. [CrossRef]
84. Chen, L.; Chen, C.; Yang, Z.; Li, S.; Chu, C.; Chen, B. Simultaneously Tuning Band Structure and Oxygen Reduction Pathway toward High-Efficient Photocatalytic Hydrogen Peroxide Production Using Cyano-Rich Graphitic Carbon Nitride. *Adv. Funct. Mater.* **2021**, *31*, 2105731. [CrossRef]
85. Kim, H.; Choi, Y.; Hu, S.; Choi, W.; Kim, J.H. Photocatalytic hydrogen peroxide production by anthraquinone-augmented polymeric carbon nitride. *Appl. Catal. B Environ.* **2018**, *229*, 121–129. [CrossRef]
86. Zhao, S.; Guo, T.; Li, X.; Xu, T.; Yang, B.; Zhao, X. Carbon nanotubes covalent combined with graphitic carbon nitride for photocatalytic hydrogen peroxide production under visible light. *Appl. Catal. B Environ.* **2018**, *224*, 725–732. [CrossRef]
87. Fu, Y.; Liu, C.; Zhang, M.; Zhu, C.; Li, H.; Wang, H.; Song, Y.; Huang, H.; Liu, Y.; Kang, Z. Photocatalytic H_2O_2 and H_2 Generation from Living Chlorella vulgaris and Carbon Micro Particle Comodified g-C_3N_4. *Adv. Energy Mater.* **2018**, *8*, 1802525. [CrossRef]
88. Li, Y.; Zhao, Y.; Wu, J.; Han, Y.; Huang, H.; Liu, Y.; Kang, Z. Photo-charge regulation of metal-free photocatalyst by carbon dots for efficient and stable hydrogen peroxide production. *J. Mater. Chem. A* **2021**, *9*, 25453–25462. [CrossRef]

89. Markovic, Z.M.; Labudova, M.; Danko, M.; Micusik, M.; Kovacova, M.; Spitalsky, Z.; Pavlovic, V.; Medic, M.; Todorovic Markovic, B.M. Highly efficient antioxidant F- and Cl-doped carbon quantum dots for bioimaging. *ACS Sustain. Chem. Eng.* **2020**, *8*, 16327–16338. [CrossRef]
90. Torres-Pinto, A.; Sampaio, M.J.; Silva, C.G.; Faria, J.L.; Silva, A.M.T. Metal-free carbon nitride photocatalysis with in situ hydrogen peroxide generation for the degradation of aromatic compounds. *Appl. Catal. B Environ.* **2019**, *252*, 128–137. [CrossRef]
91. Xie, H.; Zheng, Y.; Guo, X.; Liu, Y.; Zhang, Z.; Zhao, J.; Zhang, W.; Wang, Y.; Huang, Y. Rapid Microwave Synthesis of Mesoporous Oxygen-Doped g-C_3N_4 with Carbon Vacancies for Efficient Photocatalytic H_2O_2 Production. *ACS Sustain. Chem. Eng.* **2021**, *9*, 6788–6798. [CrossRef]
92. Lin, S.; Zhang, N.; Wang, F.; Lei, J.; Zhou, L.; Liu, Y.; Zhang, J. Carbon Vacancy Mediated Incorporation of Ti_3C_2 Quantum Dots in a 3D Inverse Opal g-C_3N_4 Schottky Junction Catalyst for Photocatalytic H_2O_2 Production. *ACS Sustain. Chem. Eng.* **2021**, *9*, 481–488. [CrossRef]